Nuclear Instruments and Methods 192 (1982) 501–511
North-Holland Publishing Company

A QUAD BGO DETECTOR AND ITS TIMING AND POSITIONING DISCRIMINATION FOR POSITRON COMPUTED TOMOGRAPHY

Hideo MURAYAMA, Norimasa NOHARA, Eiichi TANAKA
Division of Physics, National Institute of Radiological Sciences, Anagawa, Chiba-shi, 260 Japan

and

Tatsuro HAYASHI
Engineer Division, Hamamatsu TV Co., Ltd., Hamamatsu, 435 Japan

Received 31 July 1981

Quad BGO detectors and the timing and positioning discriminators have been developed for high sensitivity multilayer positron computed tomographs. Each detector consists for rectangular BGO crystals and two cylindrical photomultiplier tubes. The design allows good optical coupling between the crystals and the photomultiplier tubes, which is essential in order to obtain good time resolution with reasonable spatial resolution of the system. The discriminator consists of a time pick-off circuit based on the first photoelectron detection method and a positioning circuit. The positioning circuit identifies the crystal absorbing an annihilation photon.

The design criteria of the electronic system and the performance are described. With a suitable optical configuration of the detector, the erroneous positioning due to statistical noise is negligibly small and the coincidence time resolution for annihilation photon pairs is about 3.6 ns fwhm. The unit works satisfactorily at a count rate up to at least 360 kcps.

1. Introduction

The development of positron computed tomography and its applications in nuclear medicine have progressed very rapidly in recent years [1]. The technique makes it feasible to visualize sectional images of positron-emitting radio-pharmaceuticals given to a patient. The technique is based on the coincidence detection of annihilation photon pairs, and sectional images can be reconstructed by a computer using a similar principle to that used in X-ray computed tomography. As a result of the capability of quantitative three-dimensional imaging together with the clinical usefulness of cyclotron-produced positron emitters (^{11}C, ^{13}N, ^{15}O, ^{18}F, etc.), much effort is still being devoted to the development of systems with higher sensitivity, spatial resolution and counting speed.

A variety of devices have been designed and constructed so far. A typical detector configuration is a single- or multi-layer ring array of scintillation detectors surrounding the patient body. To attain high detection sensitivity with reasonable spatial resolution in this type of detector system, two requirements are essential: one is that a large number of small scintillators should be arranged on the ring with as high a packing ratio as possible, and the other is that the scintillators should have high stopping power for annihilation photons. Rectangular scintillation crystals are more preferable than cylindrical ones for the high packing ratio. The width of the crystals along the ring circumference limits the intrinsic spatial resolution of the obtained image, while the height of the crystal (along the detector ring axis) determines the thickness of the slice to be imaged. The width is usually chosen to be somewhat smaller than the height of the crystal, because the reconstructed images usually suffer from further smoothing in the software in order to suppress statistical noise in the images.

Bismuth germanate (BGO : $Bi_4Ge_3O_{12}$) is the most suitable scintillation material for this application because of its high gamma-ray stopping power [2], but its relatively low scintillation efficiency [8–16% of NaI(Tl)] and its long scintillation decay time (300 ns) require efficient optical coupling to photomultiplier tubes in order to obtain good time resolution and reasonable energy resolution. One-to-

0029-554X/82/0000–0000/$02.75

ton coupling between a rectangular BGO crystal and a cylindrical photomultiplier is apparently unsatisfactory for efficient optical coupling in a tightly packed multi-layer system.

A solution of this difficulty may be the use of position sensitive detector units. An example is the use of a light crystal viewed by two photomultiplier tubes, the position of scintillation in the crystal is determined from the ratio of the signal outputs of the two tubes. Ter-Pogossian and his group developed such detectors using NaI (Tl) crystals for their multi-layer systems [3–5]. In this system, 64 detector units are arranged on a circular ring, and position information in each detector is used to separate the image layers. However, this principle cannot be used for the present purpose involving the use of BGO crystals, because the poor light yield of BGO will result in insufficient positioning resolution. In addition, if we use this principle to extract position information along the detector ring circumference, misadjustment of the position-sensitive electronics may cause appreciable distortion in the images obtained.

In order to overcome these difficulties, we have constructed a quad BGO detector which is composed of four BGO crystals (trunk trapezoid and two photomultiplier tubes [6,7]. The crystal identification is performed by applying a principle similar to that employed in Ter-Pogossian's detector, but the present detector configuration provides reasonable positioning and timing properties. This detector was developed for a detector unit of a multi-layer whole-body positron computed tomograph, in which the detectors are arranged along the ring circumference of each detector ring. This paper describes the positioning property of the quad BGO detector, the timing and positioning discriminator, and the overall performance of this detector unit.

2. Principle of the quad BGO detector

The configuration of the quad BGO detector is shown in fig. 1. The BGO crystals (supplied by the Hitachi Chemical Co., Ltd.) are 15 mm wide (W), 30 mm high (H) and 24 mm long (L). Each photomultiplier tube of PMT-X and PMT-Y is an HTV R 1342 (supplied by the Hamamatsu TV Co., Ltd.) having a diameter of 29 mm (D_2). HTV R 1342 has high quantum efficiency, uniform photocathode sensitivity and small tube-to-tube variation in transit time. The two crystals C2 and C3 are optically coupled to each other with transparent silicone (silicon rubber), while the other crystals C1 and C4 are optically shielded with light reflector (BESSO) from the inner crystals. Each of the photomultiplier tubes is coupled to the two crystals with transparent silicon rubber. The other surface of the crystals are covered with the light reflector.

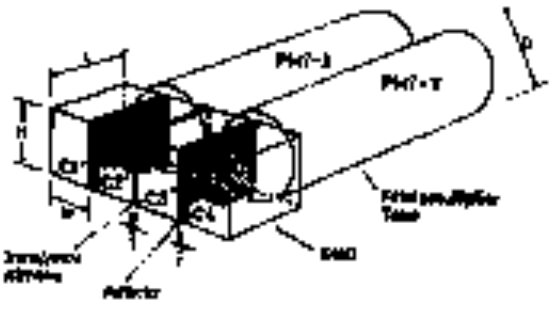

Fig. 1. Schematic drawing of the quad BGO detector.

A scintillation in one of the outer crystals produces a signal from one of the photomultiplier tubes, while that in the inner crystals yields coincident signals from the two tubes with different amplitudes. The sum of the two signals can be made almost constant whichever crystal absorbs a photon of a given energy. The scintillating crystal is identified from the relative pulse-heights of the two signals because the pulse-height ratio of the two signals largely depends on which of the crystals absorbs the photon. This is a result of the large discontinuity of the refractive index at the boundary between the inner two crystals, namely: the refractive index of the BGO crystal (n = 2.15 at 480 nm wavelength [8]) is much higher than that of the transparent silicon rubber (n = 1.45).

The positioning property is shown more clearly in fig. 2, which is a contour display of the two-dimensional pulse-height distribution of the coincident signals from the two photomultiplier tubes. Coordinates of X and Y represent the pulse-heights of the signals from PMT-X and PMT-Y, respectively. The distribution was obtained by irradiating the four crystals uniformly with a broad beam of annihilation radiations. Note that the distribution has four well separated peaks M_1 through M_4 even though the positions of the scintillations distribute randomly in the crystals.

The peaks M_1 through M_4 correspond to full energy absorption of annihilation photons in the crystals C1 through C4, respectively. The peaks M_2 and M_4 lie on the coordinate axis, while M_1 and M_3

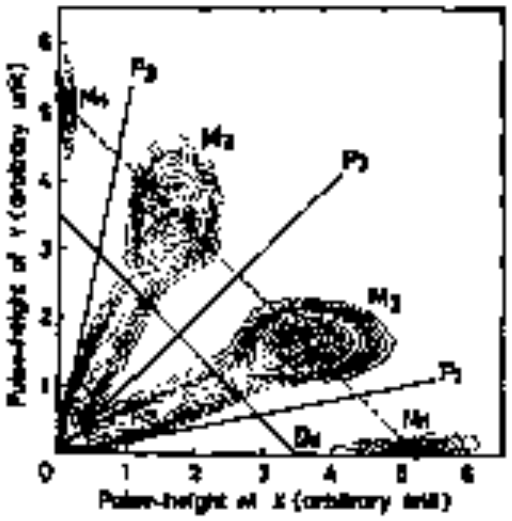

Fig. 2. Contour display of the two-dimensional pulse-height distribution of the coincident signals from the two photomultiplier tubes. Coordinates X and Y represent the pulse-heights of the signals from PMT-X and PMT-Y, respectively. The measurement was obtained by irradiating the four crystals uniformly with a broad beam of annihilation radiation.

distribute two-dimensionally. The four peaks are on a straight line (broken line) at -45° with respect to the X-axis. This implies that the sum of the signals X and Y can be used as an energy signal. The line D_0 indicates an energy discrimination level (350 keV), and three lines P_1, P_2 and P_3 represent the partitioning lines of the positioning discriminator described later. The four regions divided by the partitioning lines P_1, P_2 and P_3 are characterized by crystal addresses for the identification of the crystal absorbing the photon.

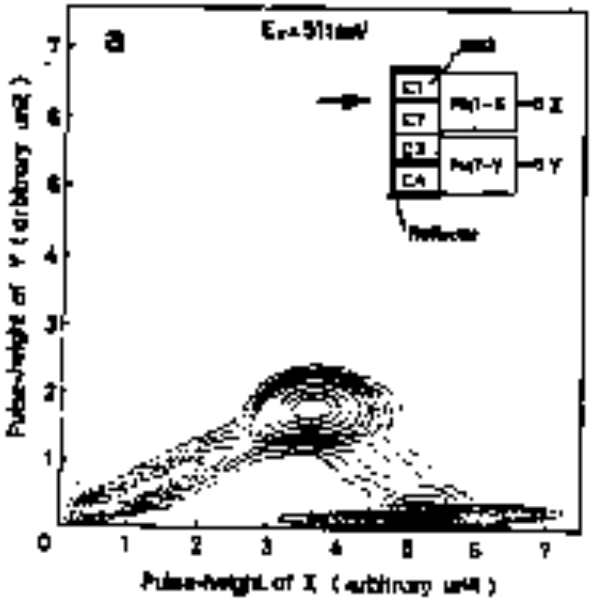

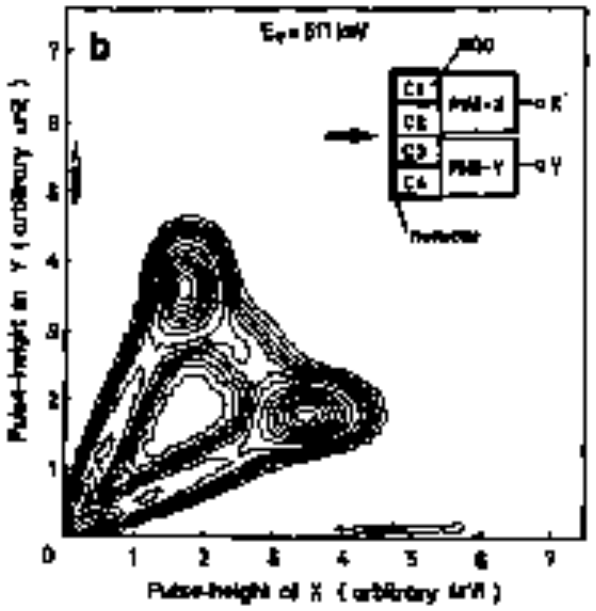

Fig. 3. Contour displays of the two-dimensional pulse-height distributions of the coincident signals from the two photomultiplier tubes. Coordinates X and Y represent the pulse-heights of the signals from PMT-X and PMT-Y, respectively. The distributions were obtained by applying a narrow beam of annihilation photons with the width of 2 mm, (a) into the boundary between the crystals C1 and C2, and (b) into the boundary between C2 and C3.

Fig. 3a is a similar result obtained by irradiating the detector with a narrow beam, 2 mm wide, at the boundary between the two crystals C1 and C2. Fig. 3b represents the result at the boundary between C2 and C3. Note that the full energy peak of the crystal C2 is located at almost the same position in both Figs. 3a and b. This fact implies that average pulse-height ratio of the signals X and Y is almost independent of the positions of scintillations in each crystal.

3. Theoretical analysis of the positioning performance

A good positioning performance of the detector is obtained with a reasonable distribution of scintillation light for the two photomultiplier tubes and the suitable setting of the partitioning lines of the positioning discriminator. We will consider the optimum condition which minimizes erroneous addresses.

Suppose that the pulse-height ratio of the coincident signals X and Y from the two photomultiplier tubes is independent of the positions of scintillations in each crystal as described above. Then, we can consider that the spreads of the full energy absorption peaks in fig. 2 mainly arise from two causes. One is the statistical fluctuation of the effective number of photoelectrons accumulated at the first dynodes of each photomultiplier tube. This arises in the successive excitation of the two adjacent crystals by a multiple interaction of a photon.

The statistical fluctuation depends on the average number of total photoelectrons, pulse-shaping in the positioning discriminator and the time when the positioning circuit is activated. The fluctuation can be represented by Poisson statistics associated with "the effective photoelectron number". The effective photoelectron number is defined by the reciprocal of the relative statistical variance of the pulse amplitude of the shaped signals in the discriminator at the time of the positioning (see Appendix).

First, we assume that the statistical spread is negligible. Then, the full energy absorption events in the individual crystals will be positioned at the maximum points of the corresponding peaks. These points are represented by M_1' through M_4' in fig. 4. The coincidence points will be on straight lines defined by

$$y = -x + NA, \tag{1}$$

where N is the sum of the effective photoelectron numbers for the X and Y signals, and A is the gain of the photomultiplier–amplifier system. The coordinates of the four points M_1' through M_4' are given by $(MA, 0)$, (M_x, M_y), (M_x, M_y) and $(0, NA)$, respectively, where

$$M_x = fNA, \quad M_y = (1-f)NA. \tag{2}$$

f ($0 < f < \frac{1}{2}$) is the distribution coefficient defined by the fraction of scintillation light received by PMT-X (or PMT-Y) for a scintillation in the crystal C3 (or C2).

The event by multiple interaction of the photon in the four adjacent crystals, however, is positioned at the intermediate point between the maximum points corresponding to the two crystals. We call such an event the cross-talk event. It can be easily shown that the position of the cross-talk event displays a line segment between the two maximum points at a ratio equal to the intensity of the absorbed energies in the individual crystals. The cross-talk events are mainly the result of photons incident near the boundary between the two crystals. The events can be seen in figs. 3a and b as each saddle between the two peaks.

To distribute the cross-talk events into the two regions equally, the partitioning line P_2 must pass through the center between the two maximum points. This is, the partitioning line P_2 must be aligned to $y = x$, while P_1 and P_3 must be aligned to $y = m^{-1}x$ and $y = mx$, respectively, where

$$m = (2-f)/f. \tag{3}$$

Next, the statistical spread of the peaks will be considered neglecting the cross-talk events. If we assume that there is no correlation between the statistical fluctuations of the two coincident signals, the distribution of the full energy absorption peak for the crystal C3, for example, is represented by a two-dimensional Gaussian function $p(x, y)$:

$$p(x,y) = \frac{1}{2\pi\sigma_x\sigma_y} \exp\left\{-\frac{1}{2}\left[\left(\frac{x-M_x}{\sigma_x}\right)^2 + \left(\frac{y-M_y}{\sigma_y}\right)^2\right]\right\}, \tag{4}$$

where

$$\sigma_x = A[fN]^{1/2}, \qquad \sigma_y = A[(1-f)N]^{1/2}. \tag{5}$$

Events positioned in the region beyond the partitioning lines P_2 and P_3 cause erroneous addresses into the other crystal addresses. We will introduce two fractions E_1 and E_2 of the wrong addresses which are defined by the functional shares of the events in the regions of $y > mx$ and $y < x$, respectively. The wrong

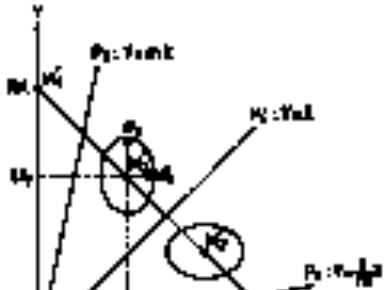

Fig. 4. Illustration of the two-dimensional pulse-height distribution of the coincident signals from the two photomultiplier tubes. Coordinates X and Y represent the pulse-heights of the signals from PMT-X and PMT-Y, respectively.

subtending fractions E_1 and E_2 are given by

$$E_1 = \frac{1}{(2\pi)^{1/2}\beta_x} \int_{-\infty}^{U_x} \exp\left(-\frac{x^2}{2\beta_x^2}\right) dx,$$

$$E_2 = \frac{1}{(2\pi)^{1/2}\beta_y} \int_{-\infty}^{U_y} \exp\left(-\frac{y^2}{2\beta_y^2}\right) dy,$$

where

$$U_x = -\frac{mM_x - M_y}{(1+m^2)^{1/2}}, \quad \beta_x = \left(\frac{m^2\sigma_x^2 + \sigma_y^2}{1+m^2}\right)^{1/2},$$

$$U_y = -\frac{M_x + mM_y}{2^{1/2}}, \quad \beta_y = \left(\frac{\sigma_x^2 + \sigma_y^2}{2}\right)^{1/2}. \tag{6}$$

Using eqs. (2), (3) and (5), we have

$$E_1 = \Phi\left[-\left(\frac{fN}{4-3f}\right)^{1/2}\right], \tag{7}$$

$$E_2 = \Phi\left[-(1-2f)N^{1/2}\right], \tag{8}$$

where $\Phi(x)$ is the Gaussian error function:

$$\Phi(x) = \frac{1}{(2\pi)^{1/2}} \int_{-\infty}^{x} \exp\left(-\frac{t^2}{2}\right) dt.$$

We define the optimum distribution coefficient f_0 which allows the larger of E_1 and E_2 to have a minimum. Considering that E_1 and E_2 are monotonically decreasing and increasing functions of f ($0 < f < \frac{1}{2}$), respectively, we can show that the optimum distribution coefficient is

$$f = f_0 = \tfrac{1}{3}. \tag{9}$$

Under this condition, $f = f_0$, we have

$$E_1 = E_2 = \Phi(-\tfrac{1}{3}N^{1/2}), \tag{10}$$

$$M_x = \tfrac{1}{3}NA, \qquad M_y = \tfrac{1}{3}NA, \tag{11}$$

$$m = 1. \tag{12}$$

Eq. (11) implies that the segment $M_1'M_4'$ is divided into three equal parts by the points M_2' and M_3'. We call this situation the optimum configuration. Eq. (12) gives lines of $y = 0.2\,x$ and $y = 5\,x$, which we call the optimum partitioning lines of P_1 and P_2.

The distribution coefficient depends on the light reflector, the size of the crystals, the refractive indexes of the crystals and the transparent adhesive, and so on. The present detector has almost the optimum configuration shown in fig. 2. The deviations of the peak points from the optimum are less than 3% of the distance between the maximum points of the outer peaks B_1 and B_4. The distribution coefficient is estimated to be about 0.31, that is $|f - f_0| \simeq 0.02$.

4. Design principles for the discriminator

The block diagram in fig. 5 represents design principles of the timing and positioning discriminator for the quad BGO detector. The discriminator is composed of two circuits. One is a time pick-off circuit and the other is a positioning discriminator.

The anode signals are summed with direct coupling of anodes of the two photomultiplier tubes, and fed to a leading-edge discriminator. It provides timing pulses with detection of the first photoelectrons in the same manner as the timing discriminator reported previously [9].

On the other hand, an energy signal is obtained by summing up the dynode signals X and Y with an analog computer ($X + Y$). The energy signal is fed to a pulse-height discriminator, the output of which is used for gating the corresponding timing pulse. Binary positioning pulses are extracted from two circuits, each of which is composed of a simple analog computer and a comparator. One is $(X - Y)$ and I_1, and the other is $[k\,\mathrm{Max}(X, Y) - (X + Y)]$ and I_2, where $\mathrm{Max}(X, Y)$ is the larger of X and Y, k is a variable constant, and I_1 and I_2 are comparators.

The former circuit corresponds to the partitioning line P_2 of $y = x$ in fig. 2, while the latter corresponds to both P_1 and P_2. The gradient m of the line P_2 is represented in terms of k as follows:

$$m = \frac{1}{2-k}. \tag{13}$$

If k is adjusted to be $\frac{5}{3}$, the lines P_1 and P_2 are aligned to the optimum partitioning lines of $y = 0.2\,x$ and $y = 5\,x$.

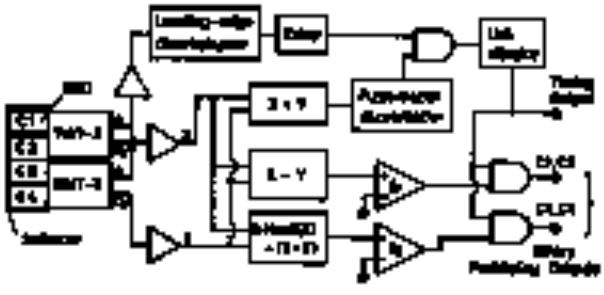

Fig. 5. Simplified block diagram of the timing and positioning discriminator for the quad BGO detector.

Fig. 6. Photographs of pulse wave forms: (a) output pulses from the analog computer ($X - Y$); (b) output pulses from the analog computer, [either $(X, Y) - (X + Y)$]; and (c) binary positioning pulses. The time scale is 500 ns/cm.

5 cm, respectively. The optimum positioning lines are shown in Fig. 2.

Photographs in figs. 6a and b are pulse waveforms of the output signals from the analog computer ($X - Y$) and [either $(X, Y) - (X + Y)$], respectively. The pulses in fig. 6a are apparently classified into four groups. These four groups from top to bottom correspond to scintillations in the individual crystals from C1 through C4, respectively. The positive and negative pulses in fig. 6b correspond to scintillations in the upper crystals of C1 and C4, and the lower crystals of C2 and C3, respectively. The comparators I_1 and I_2 divide these pulses according to their polarity.

The binary positioning pulses are derived from the output pulses from I_1 and I_2 by strobing with the timing pulses, as shown in fig. 6c. A pair of the binary positioning pulses equivalent with each timing pulse gives one of the four crystal addresses.

3. Circuit description

Fig. 7 shows a circuit diagram of the timing and positioning discriminators. The circuit was constructed to be simple and compact because it has to be provided for each detector unit and the units are closely packed on a circular geometry of a positron computed tomograph.

Current pulses from the anodes of the two photomultiplier tubes are corrected and shaped with an RC integrator (time constant 50 ns). The integrated pulse is amplified with a wide-band differential video amplifier A-1 (MC1733 with 200 MHz bandwidth and differential gain of 10). The capacitor C between pins 3 and 16 of MC1733 acts as an additional RC differentiator (time constant 150 ns) [9]. The amplified pulse is bipolar with the average zero-cross time of 250 ns and is fed to a leading-edge discriminator D-1 which is a fast ECL comparator (a half of Am687).

Two delay circuits are provided so that the energy gate pulses arrives at the gate G-2 later than the arrival of the corresponding timing pulse. One is a variable time delay which consists of an RC integrator and an ECL gate G-1. This can be used for timing adjustment for detector-to-detector variation in a range of (50 ± 6) ns. The other is a 150 ns constant delay line (15 ns rise time and 250 Ω impedance) which is contained in a dual-in-line package. The timing pulse going through the gate G-2 is fed to a multivibrator, which consists of two ECL gates G-3 and G-4. The output pulse of the multivibrator has a width of 30 ns followed by a protective dead time of 0.8 μs which is effective for eliminating pulse pile-up error.

On the other hand, the last dynode current pulse of each photomultiplier tube is shortened to a tail-pulse pulse by a delay-line clipping circuit (clipping time 150 ns), and is fed to an RC integrator (time constant 220 ns). The shortened pulses allow a good positioning performance at a high count rate. These pulses are amplified by each of the differential amplifiers A-2 and A-3 (two MC1733's with a differential gain of 100), which have an output dynamic range of 3 V with a feedback loop stabilizing a bias voltage.

The output signals from A-2 and A-3 correspond to X and Y in fig. 5, respectively. The pair of the signals X and Y is applied to the following four circuits:

(1) a couple of resistors R_1 corresponding to $(X + Y)$ in fig. 5,

(2) another couple of resistors R_2 corresponding to another $(X + Y)$ which is inverted in [either $(X, Y) - (X + Y)$],

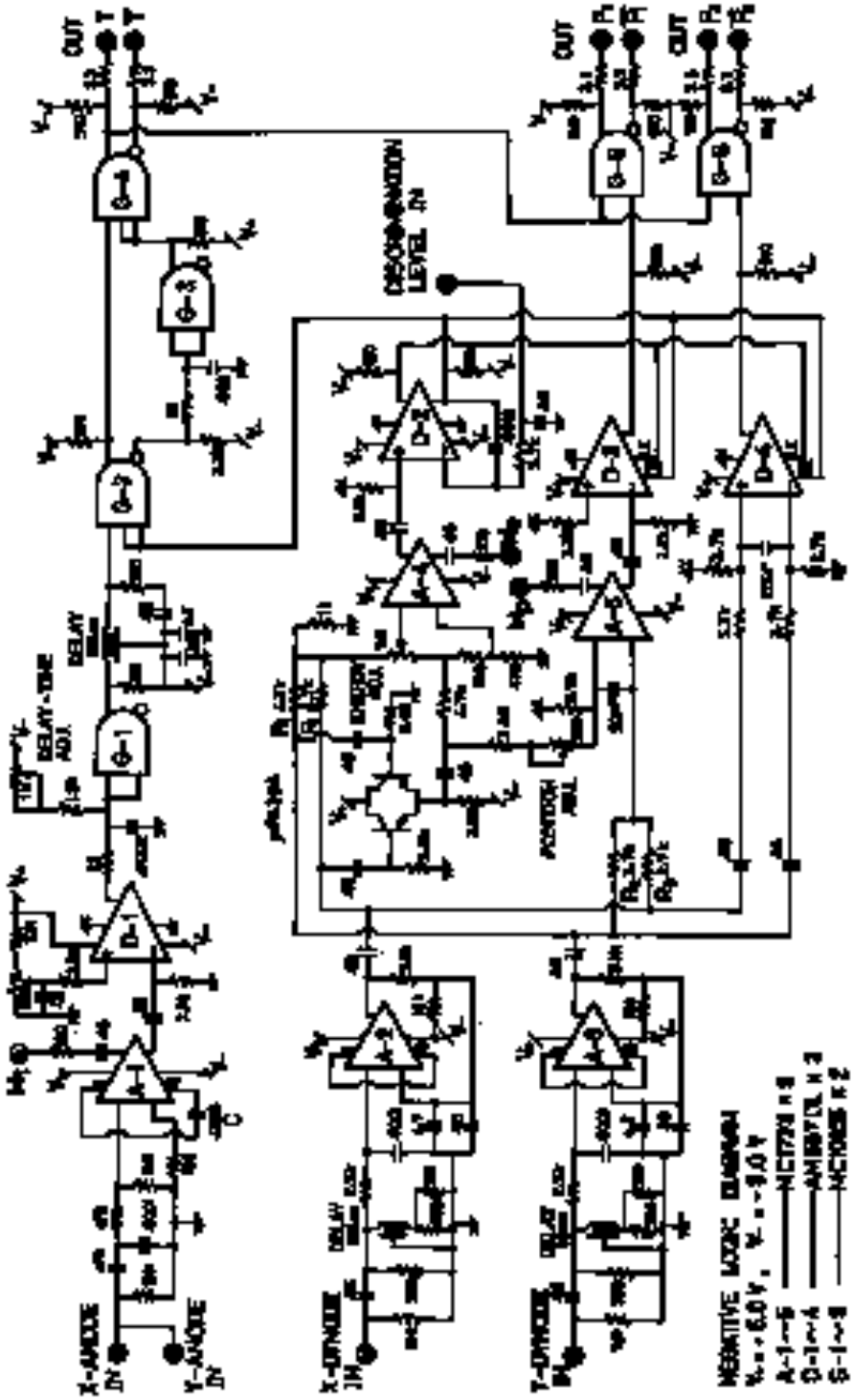

Fig. 7. Circuit diagram of the timing and positioning circuitries.

(3) a dual transistor (μPA38A) corresponding to $\mathrm{Min}(X, Y)$,

(4) a comparator D-4 (a half of Am687) corresponding to both the circuits of $(X - Y)$ and I_1.

A pulse-height correction circuit is provided for the case, in which the average pulse-height of the summed signals for the inner crystals C2 and C3 is different from that for the outer crystals C1 and C4. Such a case may be caused by the inequality of the light yield of the crystals, the inhomogeneity of the photocathode sensitivity of the photomultiplier tubes, and so on. A differential amplifier A-4 (MC1733 with a differential gain of 10) and a variable resistor ENERGY ADJ. allow the pulse-height correction to be made in the following manner.

The output signal Q from A-4 is given by

$$Q = G|pY + (1 - F)X| \qquad \text{if } X \geq Y,$$
$$Q = G|pX + (1 - F)Y| \qquad \text{if } Y > X,$$

where p is a parameter ($0 \leq p \leq 1$) adjustable with ENERGY ADJ., F is a constant of about 0.5 and G a signal gain of about 0.4. The signal Q for the inner crystals is variable with the parameter p, while Q for the outer crystals is not so. Thus, suitable adjustment of p effects both the average pulse-heights of the summed signals to be equal.

A variable resistor of POSITION ADJ. is provided for the adjustment of the parameter k in eq. (6). A differential amplifier A-5 (MC1733 with a differential gain of 10) and a comparator B-3 (a half of Am687) act as the timing comparator [either $\mathrm{Min}(X, Y) - (X + Y)$] and I_2 in fig. 5, respectively.

A pulse-height discriminator D-2 (a half of Am687) provides gate pulse for a gate G-2 and both the comparators D-3 and D-4. The comparators are unblocked during the presence of the gate pulse. Gates G-5 and G-6 allow the positioning pulse to be obtained with the corresponding timing pulse. RC integrators at input stages of A-5 and D-4 are provided for shaping the input pulses so that the positioning pulses are extracted from the gate when the shaped pulses reach the maximum (see fig. 6).

5. Experimental results

The performance of the quad BGO detector with the timing and positioning discriminators for annihilation photons was studied.

Fig. 8 shows pulse-height spectra of summed signals for the individual crystals. Each spectrum was obtained by differentiating a corresponding integral spectrum which was obtained by counting the positioning pulse as a function of the energy discrimination level. The relatively poor energy resolution of about 25% full width at half maximum (fwhm) is a result of the reduced fraction of charge integration in the circuit. Actually, experiment revealed that the energy

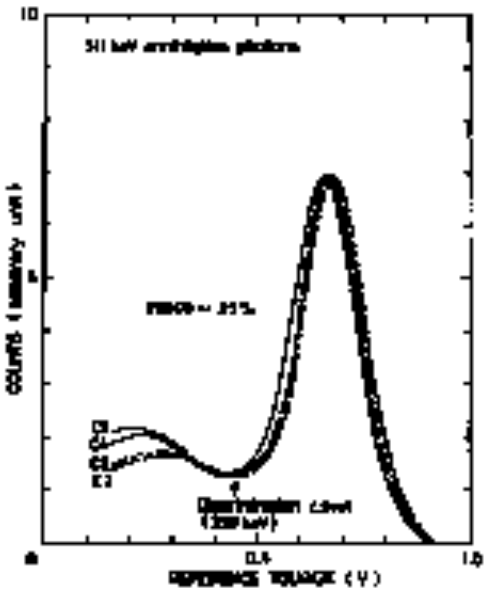

Fig. 8. Pulse-height spectra of summed signals for the individual crystals. Each spectrum was obtained by differentiating a corresponding integral spectrum which was obtained by counting the positioning pulse as a function of the energy discrimination level.

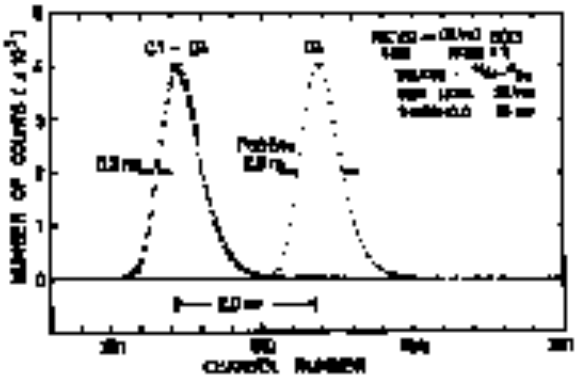

Fig. 9. Coincidence time spectra for annihilation photon pairs with the quad BGO detector and the NE102A scintillation detector. Each spectrum was obtained by gating the timing signals with the corresponding positioning signals. The difference between the two spectra of C1 provided the time resolution of 6.0 ns.

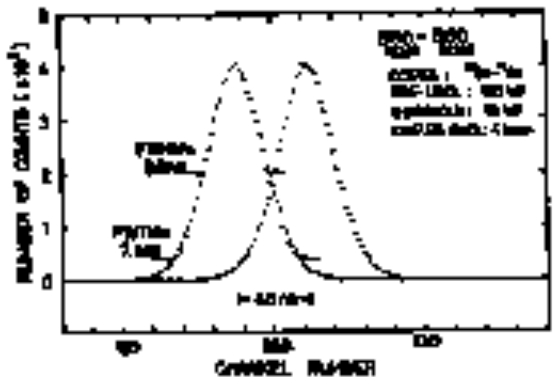

Fig. 10. Coincidence time spectra for annihilation photon pairs obtained with the two quad BGO detectors. The figures between the spectra provided the time units of 0.5 ns.

resolution was about 1.8% (wipe) when the full energy integration was achieved. The following experimental data were obtained with the energy discrimination level set at 350 keV (the minimum points of the valley of the pulse-height spectra).

Fig. 9 shows coincidence time spectra for annihilation photon pairs obtained with the detector and a time reference detector. The reference detector was a plastic scintillator NE102A (40 mm diameter × 30 mm) coupled to a 50 mm diameter photomultiplier tube (HTV R 329). The time spectrum for each crystal has the same time resolution of 2.6 ns (wipe), but is shifted in order from C2 to C4. The time difference between C1 and C4 was 0.2 ns, which corresponds to the difference in transit time between PMT-X and PMT-Y. It is negligibly small as compared with the value of 2.6 ns. Fig. 10 shows coincidence time spectra of the two quad BGO detectors. The time resolution was 3.6 ns (wipe) and 7.1 ns full width of tenth maximum (base).

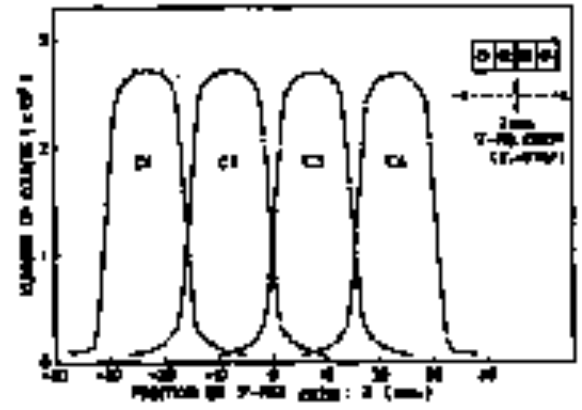

Fig. 11. Positioning responses of the quad BGO detector at a [illegible] rate of a few kcps. The responses were obtained by moving a 2 mm collimated beam of annihilation photons irradiating perpendicularly to the crystal face.

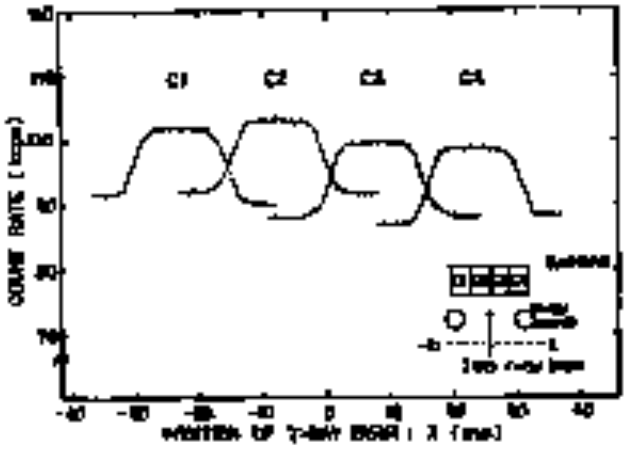

Fig. 12. Positioning responses of the quad BGO detector at a high count rate of 360 kcps (about 90 kcps for each crystal). The responses were obtained by fixing two sources ^{68}Ge–^{68}Ga in front of the detector and moving a 2 mm collimated beam of annihilation photons irradiating perpendicularly to the crystal face.

Fig. 11 shows positioning responses of the quad BGO detector at a count rate of a few kcps. The responses were obtained by moving a 2 mm collimated beam of annihilation photons irradiating perpendicularly to the crystal face. Each curve corresponds to the response of each crystal. All of the responses have a full width of 15 mm which is equal to the crystal width. Fig. 12 shows positioning responses of the detector at a high count rate of 360 kcps. The responses were obtained by fixing two sources (^{68}Ge–^{68}Ga) in front of the detector and moving a 2 mm collimated beam of annihilation photons irradiating perpendicularly to the crystal face. The differences in the peak heights were due to the different intensity and approximate centering of the two point sources.

7. Discussion and conclusion

The time resolution with detection of the first photoelectron is inversely proportional to the square root of total photoelectrons N_0 [9]. The positioning property, however, depends on the effective photoelectron number N.

The values of N_0 and N can be estimated from measurements of energy resolutions with different integration time constants [10]. The relative total variance V_T of the pulse-height for a mono-energetic spectrum is given by

$$V_T = V_S + V_C,$$

where V_S is the relative statistical variance and V_C the relative non-statistical variance. The latter is caused by the inevitable nonuniformity of the scintillation crystal, inhomogeneity of the photocathode of the photomultiplier tube, and so on. Since the relative statistical variance is given by the reciprocal of the effective photoelectron number, we have

$$V_T = \frac{1}{N} + V_C . \tag{14}$$

For the full charge integration, we have another value of the relative total variance V_{T_0}:

$$V_{T_0} = \frac{1}{N_0} + V_C . \tag{15}$$

On the other hand, the effective photoelectron number in pulse-charging with an RC integration (time constant T_1) at time t is given by

$$N = \frac{T_1(2\tau - T_1)(e^{-t/\tau} - e^{-t/T_1})^2}{(\tau - T_1)^2(e^{-2t/\tau} - e^{-2t/T_1})} N_0 , \tag{16}$$

where τ is the decay time constant of scintillation (see Appendix). Thus, we can determine N_0, N and V_C from eqs. (14), (15) and (16) using the experimental values of V_T and V_{T_0}.

From the experimental results of the energy resolution of 25% with the positioning discriminator and 18% for the full charge integration, we have $V_T = 0.0113$ and $V_{T_0} = 0.0059$. Since the positioning discriminator has $T_1 = t = 220$ ns and $\tau = 300$ ns, eq. (16) gives $N = 0.47\,N_0$. Then, we obtain

$$N_0 = 210, \tag{17}$$
$$N = 99, \tag{18}$$
$$V_C = 0.0039. \tag{19}$$

In the previous experiment using a single BGO crystal [9], it was shown that the BGO–BGO coincidence time resolution ΔT (ns) in FWHM is approximately given by

$$\Delta T = 780/N_0. \tag{20}$$

Eq. (20) with $N_0 = 210$ gives $\Delta T = 3.7$ ns, which is consistent with the present experimental time resolution (3.6 ns).

From the estimated value of $N = 99$, the erroneous addressing due to the statistical noise can be evaluated. If the detector has the optimum distribution coefficient ($f = f_0 = \frac{1}{2}$), the wrong addressing fractions are obtained to be $\mathcal{E}_1 = \mathcal{E}_2 = 0.0478$ using eq. (10). The larger of $\mathcal{E}_1$ and $\mathcal{E}_2$ increases with the increase of $|f - f_0|$, but it is estimated to be less than 1% even for $|f - f_0| = 0.05$ using eqs. (7) and (8). Since the detector has $|f - f_0| = 0.02$, the wrong addressing is negligible.

The value of $N = 99$ gives the relative statistical variance:

$$V_S = 0.01. \tag{21}$$

In comparison with eqs. (19) and (21), V_C is much smaller than V_S. It corresponds to the fact that the signals X and Y from the two photomultiplier tubes have negligible correlation, which supports the assumption used in the derivation of eq. (4).

The response curves in fig. 10 display a relatively positioning property except that the tails of the peaks overlap with the adjacent peaks. These tails arise from the inevitable cross-talk events due to the multiple interaction of photons. The experimental result in fig. 12 suggests that the detector tech has a normal positioning property at the high count rate of 360 kcps (about 90 kcps for each crystal). The good count-rate performance ensures that the detector units are suitable for dynamic studies with positron computed tomographs.

This work was carried out as a part of the National Project on Whole-Body Positron Tomographs supported by the Agency of Industrial Science and Technology, the Ministry of International Trade and Industry, Japan. The photomultiplier HTV R 1353 was developed for the project.

We gratefully acknowledge those engaged in the project, in particular Drs. K. Takami and K. Ishimaru, and Messrs. H. Nakase and K. Okajima for their helpful discussions. We wish to express appreciations to Messrs. K. Futatsuka, T. Tomiyori and M. Yamamoto for their useful suggestions and discussions. Finally, we wish to acknowledge the support of the Grant-in-Aid for Cancer Research (55–17) from the Ministry of Health and Welfare, Japan.

Appendix: Effective photoelectron number in pulse-shaping with an RC integrator

The average shape of the original scintillation current pulses for photons of a given energy can be described in terms of photoelectron numbers arriving at the first dynode of the photomultiplier tube in unit time, as follows:

$$I(t) = \frac{N_0}{\tau}\, e^{-t/\tau}\, U(t), \tag{A1}$$

where τ is the decay time constant of scintillation, N_0 the average number of total photoelectrons and $U(t)$ the step function.

When the original pulses are shaped with an RC integrator (time constant T_1), the average pulse waveform $\bar{V}(t)$ is given by

$$\bar{V}(t) = \int_{-\infty}^{\infty} I(x)\, s(t-x)\, dx, \tag{A2}$$

where $s(t)$ is the response function of the circuit, given by

$$s(t) = \frac{1}{T_1}\, e^{-t/T_1}. \tag{A3}$$

Owing to the statistical fluctuation of the photoelectrons accumulated, the individual pulse-amplitude $V(t)$ fluctuates from $\bar{V}(t)$. The standard deviation $\Delta V(t)$ is represented by

$$[\Delta V(t)]^2 = \int_{-\infty}^{\infty} I(x)\,[s(t-x)]^2\, dx. \tag{A4}$$

Therefore, the relative statistical variance of the integrated pulse-amplitude at time t is

$$\left[\frac{\Delta V(t)}{\bar{V}(t)}\right]^2 = \frac{1}{N_0}\,\frac{(\tau - T_1)^2(e^{-t/\tau} - e^{-2t/T_1})}{T_1(2\tau - T_1)(e^{-t/\tau} - e^{-t/T_1})^2}. \tag{A5}$$

The reciprocal of the variance gives the effective photoelectron number expressed by eq. (16).

References

[1] T.F. Budinger, S.E. Derenzo, G. Gullberg and R. Huesman, IEEE Trans. Nucl. Sci. NS-26 (1979) 2742.

[2] Z.H. Cho and M.R. Farukhi, J. Nucl. Med. 18 (1977) 840.

[3] M.M. Ter-Pogossian et al., Radiology 128 (1978) 477.

[4] M.M. Ter-Pogossian et al., J. Comput. Assist. Tomogr. 2 (1978) 539.

[5] N.A. Mullani et al., IEEE Trans. Nucl. Sci. NS-25 (1978) 781.

[6] N. Nohara et al., Proc. 3rd Symp. on Physical and technical aspects of CT, Tokyo, (September, 1980) p. 39.

[7] H. Hayashi et al., Proc. 3rd Symp. on Physical and technical aspects of CT, Tokyo (September, 1980) p. 95.

[8] G.H. Moore and C.V. Hollis, IEEE Trans. Nucl. Sci. NS-23 (1976) 56.

[9] H. Mitzushima, Nucl. Instr. and Meth. 177 (1980) 453.

[10] P. Ott and H.P. Bell, Nucl. Instr. and Meth. 17 (1962) 69.